scientific reports

Check for updates

OPEN

Information theory and thermal properties of an extended cosine hyperbolic potential model

Chou-Yi Hsu[6], Pradeep Kumar Singh[7]✉, Yusufbay Yusupov[8], Doniyor Jumanazarov[9], Ibrahim Mahariq[1,2,3,4,5], Ali A. Rajhi[10] & Makus Ahmes[11]✉

This study presents the information-theoretic measures and molar thermodynamic properties for an extended cosine hyperbolic potential. The analytic expressions for the Fisher information in both position and momentum spaces are derived. The Shannon entropy for both position and momentum spaces are also derived. The Cramér-Rao bound and Beckner-Bialynicki-Birula-Mycielski (BBM) inequality are tested and confirmed, presenting the model as a good fit for the study of information theory. The study of thermodynamic properties is applied to phosphorus (P_2), potassium (K_2), potassium bromide (KBr), and silicon monoxide (SiO) molecules using specific analytical equations. The results for molar enthalpy (H), molar entropy (S), molar Gibbs free energy (G), and molar heat capacity (C_p) for the four molecules across a temperature range of 0 K to 6000 K are numerically obtained. The predicted results demonstrate excellent consistency with experimental data obtained from the National Institute of Standards and Technology (NIST) database. The discrepancies observed indicate minor variations in the model's accuracy, providing reliable predictions for the molar thermodynamic properties of the molecules. The performance of the model validates its suitability for studying information theory and accurately representing thermal properties.

Keywords Thermal properties, Molar entropy, Fisher information, Shannon entropy, Molar enthalpy

The development of information theory by Claude Shannon provides a mathematical framework that quantifies, encodes, transmits, and analyzes information, addressing the fundamental limits of data compression and communication accuracy[1–3]. This information theory is critically studied in the science as a quantitative way of assessing the content of information in a system or probability distribution. In physics and quantum mechanics, it helps to analyze uncertainty, complexity, and the structure of wave functions or probability distributions. The most powerful concepts in information-theoretic measures are Fisher information and Shannon entropy. Fisher information quantifies the sensitivity of a probability distribution to small changes in its parameters. It is widely used in quantum mechanics to study the localization of wave functions. Shannon entropy, on the other hand, measures the average uncertainty, accounting for the information content of a probability distribution. In recent developments, Shannon entropy and Fisher information have emerged as powerful tools for analyzing diatomic molecules, offering insights beyond conventional observables like energy and angular momentum. Shannon entropy captures the overall spread of the electronic density, while Fisher information highlights local variations and sharp features. Studies using analytically solvable potentials like the Deng-Fan-Eckart models[4] show that these measures reflect electron localization, delocalization, and molecular confinement, and satisfy key uncertainty relations. By complementing traditional quantum and spectroscopic analyses, information-theoretic approaches provide a nuanced understanding of chemical bonding, electron correlations, and the response of molecules to external fields, establishing a versatile framework for probing molecular structure and

[1] College of Engineering and Architecture, Gulf University for Science and Technology, Mishref, Kuwait. [2]Department of Electrical and Electronic Engineering, Faculty of Engineering and Architecture, Istanbul Gelisim University, 34310, Avcılar-Istanbul, Türkiye. [3] Najjad Zeenni Faculty of Engineering, Al-Quds University, Jerusalem, Palestine. [4]Department of Medical Research, China Medical University Hospital, China Medical University, Taichung, Taiwan. [5]University College, Korea University, Seoul 02481, South Korea. [6]Thunderbird School of Global Management, Arizona State University, Tempe Campus, Phoenix, AZ 85004, USA. [7]Department of Mechanical Engineering, Institute of Engineering & Technology, GLA University, Mathura 281406, Uttar Pradesh, India. [8]Kimyo International University in Tashkent, Shota Rustaveli str. 156, Tashkent 100121, Uzbekistan. [9]Urgench State University, Kh. Alimdjan str. 14, Urgench 220100, Uzbekistan. [10]Department of Mechanical Engineering, College of Engineering, King Khalid University, Abha 61421, Saudi Arabia. [11]Department of Physics, Salem University Lokoja, Kogi, Nigeria. ✉email: pradeep.kumar@gla.ac.in; makusamhes@gmail.com

dynamics[5–7]. These theoretical measures can be calculated from the solutions of the energy levels/wave functions. The energy levels serve as a foundation for the computation of many quantities in quantum mechanics, including thermodynamic properties. The importance of thermodynamic properties as physical quantities in science and engineering cannot be overstated. These properties are crucial for understanding, developing, and improving processes across diverse scientific and engineering disciplines. They provide vital insights into the energy, stability, and behaviour of substances under different conditions. These quantities have significantly enhanced the understanding of phenomena such as fluorescence microscopy, protein activity, phase transitions, material synthesis, dissolution, and adsorption[8–12]. The thermal properties include molar entropy, molar enthalpy, molar Gibbs free energy, and molar heat capacity. Different authors have reported these properties individually or collectively under different potential models[13,14]. In Ref[15]., Eyube et al. reported the molar enthalpy and molar Gibbs free energy for three different molecules. These authors employed the improved Pöschl-Teller oscillator to obtain the energy levels. The two properties were calculated using the Poisson summation formula. The calculated results of the three models showed little deviation from the observed results. The authors reported deviations of 0.8178%, 3.1939%, and 0.5312% for molar enthalpy of P_2, N_2, and ICl molecules, respectively. They also reported deviations of 0.3865%, 0.4360%, and 0.405% for the molar Gibbs free energy of P_2, N_2, and ICl gaseous molecules. Emeje et al.[16] reported the molar enthalpy, heat capacity at constant pressure, and molar Gibbs free energy of nitrogen and iodine molecules for a modified shifted Morse potential function. These authors examined the thermal properties of their proposed model over a temperature range of 0 K to 6000 K. The results were found to align with the observed results in the NIST database. To assess the accuracy of their results, they calculated the absolute average percentage deviation of the calculated results from the observed results. Their study reported percentage deviations of 0.031% and 0.034% for molar enthalpy of I_2 and N_2, respectively. They also reported deviations for molar heat capacity and molar Gibbs free energy as 0.073%, 0.153%, and 0.032%, 0.008% for I_2 and N_2, respectively. Similarly, Horchani and Jelassi[17] reported the molar entropy of CsO, CsF, and CsCl molecules for the improved Tietz oscillator. The authors provided the full equation for the energy levels of the improved Tietz oscillator and used it to calculate the vibrational partition function. The calculated results were presented graphically in comparison with observed data. To assess the accuracy of their model, they calculated the percentage deviation of the analytical results from the observed results, reporting deviations of 0.228%, 0.267%, and 0.284% for CsO, CsF, and CsCl, respectively.

In another study, Horchani et al.[18] reported the molar enthalpy of CsO, CsF, and CsCl for the shifted Tietz-Wei potential model. The authors first obtained solutions of the radial Schrödinger equation for their model. The molar enthalpy was then studied in detail by deriving expressions to generate values for comparison. The calculated results for the three molecules agreed with the observed results. The average relative deviations were reported as 1.72%, 1.52%, and 2.86% for CsO, CsF, and CsCl, respectively. Jia et al.[19] reported the molar entropy and molar Gibbs free energy of the nitrogen dimer for a modified Rosen-Morse oscillator. Without providing the energy levels of the modified Rosen-Morse potential, the authors derived the vibrational partition function and used it to compute expressions for entropy and Gibbs free energy. Using contributions from rotational, translational, and vibrational entropies and Gibbs free energy, the authors calculated molar entropy and molar Gibbs free energy for the modified Rosen-Morse potential. Their results showed that these quantities can be accurately predicted for temperatures from 0 K to 6000 K. In Ref[20]., the molar entropy of I_2, SiC, CP, and F_2 molecules for the modified shifted Morse potential were reported. The authors explicitly calculated the expression for molar entropy and generated numerical values, which agreed with observed results with minimal differences. The reported percentage deviations were 0.012%, 0.004%, 0.004%, and 0.010% for I_2, CP, F_2, and SiC, respectively. Recently, Onate et al.[21] calculated molar enthalpy and molar heat capacity at constant pressure for F_2, I_2, CsO, and CsF molecules for the symmetric trigonometric Rosen-Morse plus Pöschl-Teller potential. Their model reproduced results with smaller percentage deviations.

Following the above and other literature, it is evident that different models yield different results for any given molecule. Thus, it is important to identify a model with minimal percentage deviation[22,23]. Motivated by the interest in theoretical quantities and molar thermal properties for molecular systems, this study examines Fisher information, Shannon entropy, and molar thermodynamic properties of an extended cosine-hyperbolic-type potential function for several molecules. The extended cosine-hyperbolic-type potential is mathematically written as[24]

$$V(r) = V_1(V_0\cosh(\alpha r) + V_0\sinh(\alpha r) - 1)^2. \tag{1}$$

In Eq. (1), the parameters $V_0$and $V_1$are potential parameters that defines the applications of the potential. To study this potential for different molecules, we followed the condition for diatomic molecular potential energy function as[24]

$$\left.\begin{aligned} \frac{dV(r}{dr}\bigg|_{t=r_e} &= 0, \\ V(\infty) - V(r_e) &= V_1, \\ \frac{d^2V(r)}{dr^2} &= 4\mu\pi^2c^2\omega_e^2 \end{aligned}\right\}. \tag{2}$$

From the Eq. (2), $\alpha$is given as

$$\alpha = c\pi\omega_e\sqrt{\frac{2\mu}{V_1V_0^2}}, \tag{3}$$

where c is the speed of light, $\mu$is the reduced mass of the particle, $V_1$is the dissociation energy and $\omega_e$the harmonic vibrational frequency. The extended cosine hyperbolic type potential has energy levels of the form[24]

$$E_v = V_1 - \frac{\alpha^2\hbar^2}{2\mu}\left(\frac{1}{\alpha\hbar}\sqrt{2\mu V_1} - \frac{1}{2} - v\right)^2, \tag{4}$$

and the radial wave function as.

$$R(y) = Ny^u e^{-\eta y}L_n^u(2\eta y), y = e^{\alpha r} \tag{5}$$

where,

$$u = \sqrt{\frac{2\mu(V_1 - E_v)}{\alpha^2\hbar^2}}, \eta = \sqrt{\frac{2\mu V_1V_0^2}{\alpha^2\hbar^2}} \tag{6}$$

Theoretic measures

The section deals with the computations of the theoretic measures. The major theoretic measure to be studied in the work are Fisher information and Shannon entropy. These two quantities have been examined under different models where the characteristics of the models' parameters on the quantities are verified[25–27].

Fisher information

Fisher information for both position space and momentum space respectively are given as[28–30]

$$\left.\begin{aligned} I(\rho) &= \int \frac{1}{\rho(r)}\left(\frac{d\rho(r)}{dr}\right)^2 dr \\ I(\gamma) &= \int \frac{1}{\gamma(p)}\left(\frac{d\gamma(p)}{dp}\right)^2 dp \end{aligned}\right\}, \tag{7}$$

where $\gamma(p)$and $\gamma(p)$are probability densities for position and momentum spaces respectively. The Fisher information for the position space can be obtained using the wave function in Eq. (7) but the Fisher information for the momentum can be obtained by taking the Fourier transform of the radial wave function. Thus, in the momentum space, we relate the probability density and the wave function as

$$\gamma(p) = |\Phi(p)|^2, \tag{8}$$

where $\Phi(p)$is the Fourier transform of $R(r)$. With the position probability density, a transformation of the form $y = e^{\alpha r}$,and a derivative as

$$\frac{d\rho(y)}{dy} = N^2\left(2uy^{2u-1}e^{-2\eta y} - 2\eta y^{2u}e^{-2\eta y}\right), \tag{9}$$

the Fisher information for the position space becomes

$$I(\rho) = 4\alpha N^2\left[u^2\int_0^\infty y^{2u-3}e^{-2\eta y}dy - 2u\eta\int_0^\infty y^{2u-2}e^{-2\eta y}dy + \eta^2\int_0^\infty y^{2u-1}e^{-2\eta y}dy\right]. \tag{10}$$

Using integral of the form

$$\int_0^\infty x^n e^{-ax}dx = \frac{\Gamma(n+1)}{a^{n+1}}, \tag{11}$$

The Fisher information for the position space finally becomes

$$I(\rho) = \frac{2\alpha\eta(2\eta)^{2u}n!}{\Gamma(u+\eta+1)}\left[\frac{u^2\Gamma(2u-2)}{(2\eta)^{2u-2}} - \frac{2u\eta\Gamma(2u-1)}{(2\eta)^{2u-1}} + \frac{\eta^2\Gamma(2u)}{(2\eta)^{2u}}\right]. \tag{12}$$

For the momentum space,

$$\frac{d\gamma(p)}{dp} = 4N^2\,(u+1) \times \frac{2\gamma^2 p}{\left(\eta^2+\gamma^2p^2\right)^{u+2}}, \tag{13}$$

where $\gamma = (\hbar\alpha)^{-1}$.Then,

$$I(\gamma) = 4N^2(u+1)^2\gamma^4 \int_{-\infty}^{\infty} \frac{p^2}{\left(\eta^2+\gamma^2p^2\right)^{u+3}}dp. \tag{14}$$

With change of variable of the form $x = \gamma p$,

$$I(\gamma) = 4N^2(u+1)^2\gamma^2 \int_{-\infty}^{\infty} \frac{x^2}{\left(\eta^2+x^2\right)^{u+3}}dx. \tag{15}$$

Using integral of the form

$$\int_{-\infty}^{\infty} \frac{a^2}{\left(x^2+a^2\right)^n}da = \frac{\pi b^{3-2n}(n-3/2)}{(n-1)(n-2)}. \tag{16}$$

Then, we have

$$I(\gamma) = \frac{4(u+1)\eta^{2u+1}\Gamma(u+1)}{\hbar^2\alpha^2\sqrt{\pi}\Gamma(u+1/2)} \times \frac{\pi\eta^{-(2u+3)}(u+3/2)}{(u+2)}. \tag{17}$$

Shannon entropy
The Shannon entropy for both the position space and momentum space respectively are given as[31,32]

$$\left.\begin{aligned} S(\rho) &= \int \rho(r)\ln\rho(r)dr, \\ S(\gamma) &= \int \gamma(p)\ln\gamma(p)dp \end{aligned}\right\}. \tag{18}$$

In the position space where $\rho(r) = |R(y)|^2$, the Shannon entropy becomes

$$S(\rho) = -\int_0^{\infty} \rho(y)\ln\rho(y)\frac{1}{\alpha y}dy. \tag{19}$$

Substituting for the probability density, the above equation becomes

$$S(\rho) = -\frac{N^2}{\alpha}\left[\ln N^2 \int_0^{\infty} y^{2u-1}e^{-2\eta y}dy + 2u\int_0^{\infty} y^{2u-1}\ln y e^{-2\eta y}dy - 2\eta\int_0^{\infty} y^{2u}e^{-2\eta y}dy\right]. \tag{20}$$

Defining an integral of the form

$$\left.\begin{aligned} \int_0^{\infty} x^n e^{-ax}dx &= \frac{\Gamma(n+1)}{a^{n+1}}, \\ \int_0^{\infty} x^n \ln x.e^{-ax}dx &= \frac{\Gamma(n+1)\left[\psi(n+1)-\ln a\right]}{a^{n+1}} \end{aligned}\right\}. \tag{21}$$

The analytic equation for the position space Shannon entropy becomes

$$S(\rho) = \frac{2\eta(2\eta)^{2u}n!}{\Gamma(u+\eta+1)}\left[\ln\frac{2\alpha\eta(2\eta)^{2u}n!}{\Gamma(u+\eta+1)}\frac{\Gamma(2u)}{(2\eta)^{2u}} + \frac{2u\Gamma(2u)\left[\psi(2u)-\ln(2\eta)\right]}{(2\eta)^{2u}} - \frac{2\eta\Gamma(2u+1)}{(2\eta)^{2u+1}}\right]. \tag{22}$$

In the momentum space, where the Fourier transform of $R(y)$is considered, the Shannon entropy becomes

$$S(\gamma) = N^2(u+1)\int_{-\infty}^{\infty} \frac{\ln(\eta^2+\gamma^2p^2)}{\left(\eta^2+\gamma^2p^2\right)^{u+1}}dp - \ln N^2 \int_{-\infty}^{\infty} \frac{\ln N^2}{\left(\eta^2+\gamma^2p^2\right)^{u+1}}dp. \tag{23}$$

On simplifying the integral following previous steps, the analytic equation for the momentum Shannon entropy becomes

$$S(\gamma) = (u+1)\left[\ln \eta^2 - \psi(u+1/2) + \psi(u+1)\right] - \ln \frac{\eta^{2u+1}\Gamma(u+1)}{\hbar\alpha\sqrt{\pi}\Gamma(u+1/2)}. \tag{24}$$

The partition function

The computation of the thermodynamic properties relies on the partition function[33,34]. The partition function is a tool used to express the relevant thermodynamic functions such as the S, H, G and C_p. For molar thermodynamic properties, the molar partition function is a contribution of the vibrational part, rotational part and translational part. These three-partition functions will be given one after the other.

Vibrational partition function

The vibrational partition function is given as[35–53]

$$Q_v = \sum_{\nu=0}^{\nu \max} \mathrm{e}^{-\beta E_\nu}, \tag{25}$$

where $\beta = 1/k_B T$, k_B is the Boltzmann constant, T is the absolute temperature and ν_{max} is the upper bound vibrational quantum number obtained from the first derivative of the energy level. By expression, the upper bound vibrational quantum state for Eq. (4) is

$$\nu_{\max} = \frac{1}{2}\left(1 + \frac{2\sqrt{2\mu V_1} - 2\alpha\hbar}{\alpha\hbar}\right) \tag{26}$$

.

Following the energy levels in Eq. (4), Eq. (5) turns out to be

$$Q_v = \mathrm{e}^{-\beta V_1} \sum_{\nu=0}^{\nu \max} \mathrm{e}^{\beta \frac{\alpha^2\hbar^2}{2\mu}\left(\frac{1}{\alpha\hbar}\sqrt{2\mu V_1} - \frac{1}{2} - v\right)^2}. \tag{27}$$

To evaluate the summation in Eq. (27), it is convenient to use the modified Poisson summation formula[54,55] which is accurate and simple as it gives the approximate value of the summation. The study will consider the lowest order approximation. Thus, the quantum correction terms will not be considered. The summation in Eq. (27) can then be written as

$$Q_v = \sum_{\nu=0}^{\nu \max} \mathrm{e}^{\beta \frac{\alpha^2\hbar^2}{2\mu}\left(\frac{1}{\alpha\hbar}\sqrt{2\mu V_1} - \frac{1}{2} - v\right)^2} = \sum_{\nu=0}^{\nu \max} f(v). \tag{28}$$

Equation (28) can be simplified using the formula

$$Q_v = \sum_{\nu=0}^{\nu \max} f(v) = 0.5\left\{f(0) - f(v_{\max}+1)\right\} + \int_0^{v \max+1} f(x)dx. \tag{29}$$

In other to evaluate the definite integral in Eq. (29), we define a variable of the form $\Phi_1 = \Phi_0\left\{\alpha^{-1}\hbar^{-1}\sqrt{2\mu V_1} - 2^{-1} - x\right\}$,where $\Phi_0 = \alpha\hbar\sqrt{(2\mu)^{-1}\beta}$.Using the transformation and input Eq. (28) into Eq. (29), we have

$$Q_v = 0.5\left\{e^{\Phi_2^2} - e^{\Phi_0^2}\right\} - \frac{1}{\Phi_0}\int_{\Phi_3}^{-\Phi_0} e^{\Phi_1^2} d\Phi_1, \tag{30}$$

where we have used the following for simplicity.

$$\Phi_2^2 = \frac{\beta\alpha^2\hbar^2}{2\mu}\left(\frac{1}{\alpha\hbar}\sqrt{2\mu V_1} - \frac{1}{2}\right)^2, \quad \Phi_3 = \Phi_0 v_{mx} \tag{31}$$

Equation (30) can fully be simplified to obtain the complete vibrational partition function using maple software program to have

$$Q_v = \frac{e^{-\beta V_1}}{2}\begin{bmatrix} e^{\frac{\beta\alpha^2\hbar^2}{2\mu}}\left\{e^{\left(\frac{1}{\alpha\hbar}\sqrt{2\mu V_1}-\frac{1}{2}\right)^2}-1\right\}+\frac{\sqrt{\pi}}{\alpha\hbar\sqrt{\frac{\beta}{2\mu}}}erfi\left(\alpha\hbar\sqrt{\beta(2\mu)^{-1}}\right) \\ +\frac{\sqrt{\pi}}{\alpha\hbar\sqrt{\frac{\beta}{2\mu}}}erfi\left(\frac{1}{2}\left(1+\frac{2\sqrt{2\mu V_1}-2\alpha\hbar}{\alpha\hbar}\right)\alpha\hbar\sqrt{\beta(2\mu)^{-1}}\right) \end{bmatrix}. \tag{32}$$

The rotational and translation partition functions

By regarding a diatomic molecule as a rigid rotor, and neglecting the interactions of the molecules as it is considered to be very weak, the rotational partition function and translational partition function respectively are given as

$$Q_r = \frac{T}{\tau\Theta}\left\{1+\frac{1}{3}\frac{\Theta}{T}+\frac{1}{15}\left(\frac{\Theta}{T}\right)^2+\frac{4}{315}\left(\frac{\Theta}{T}\right)^3\right\}, \tag{33}$$

$$Q_t = \left(\frac{2\pi m k_\beta T}{h^2}\right)^{\frac{3}{2}}V, \tag{34}$$

where V is the volume of the gas, m is the mass of the gas molecule, $\Theta = h^2\left(8\mu k_\beta\pi^2 r_e^2\right)^{-1}$is the rotational characteristic temperature and τtakes the value 1 and 2 for heteronuclear and homonuclear molecules respectively. The total partition function is the product of Eqs. (12), (33) and (34). Thus

$$Q = Q_v Q_r Q_t. \tag{35}$$

The thermodynamic properties

At this point, the various thermodynamic properties can now be calculated. It should be noted that the experimental values for each of the molar thermodynamic property is a combination of three contributions from the vibrational, rotational and translational parts.

Enthalpy: The molar enthalpy H is the sum of the vibrational enthalpy H_v the rotational enthalpy H_r and the translational enthalpy H_t given as

$$H = H_v + H_r + H_t, \tag{36}$$

where

$$\begin{aligned} H_v = {} & \frac{V_1 e^{0.5\beta\mu^{-1}\alpha^2\hbar^2}\left[e^{\left(\alpha^{-1}\hbar^{-1}\sqrt{2\mu V_1}-0.5\right)^2}-1\right]-\left[\alpha^2\hbar^2\mu^{-1}\beta T^{-1}e^{0.5\beta\mu^{-1}\alpha^2\hbar^2}\left\{e^{\left(\alpha^{-1}\hbar^{-1}\sqrt{2\mu V_1}-0.5\right)^2}-1\right\}\right]}{e^{0.5\beta\mu^{-1}\alpha^2\hbar^2}\left(e^{\left((\alpha\hbar)^{-1}\sqrt{2\mu V_1}-0.5\right)^2}-1\right)+\frac{\sqrt{2\pi}\left[erfi\left(0.5\alpha\hbar\sqrt{2\beta\mu^{-1}}\right)+erfi\left(\left(0.5(\alpha\hbar)^{-1}\sqrt{2\mu V_1}-1\right)\alpha\hbar\mu^{-1}\sqrt{2\beta}\right)\right]}{\alpha\hbar\sqrt{\beta\mu^{-1}}}} \\ & +\frac{\frac{\sqrt{2\pi}\left[erfi\left(0.5\alpha\hbar\sqrt{2\beta\mu^{-1}}\right)+erfi\left(\left(0.5(\alpha\hbar)^{-1}\sqrt{2\mu V_1}-1\right)\alpha\hbar\mu^{-1}\sqrt{2\beta}\right)\right]}{\mu\left(\beta\mu^{-1}\right)^{3/2}}}{e^{0.5\beta\mu^{-1}\alpha^2\hbar^2}\left(e^{\left((\alpha\hbar)^{-1}\sqrt{2\mu V_1}-0.5\right)^2}-1\right)+\frac{\sqrt{2\pi}\left[erfi\left(0.5\alpha\hbar\sqrt{2\beta\mu^{-1}}\right)+erfi\left(\left(0.5(\alpha\hbar)^{-1}\sqrt{2\mu V_1}-1\right)\alpha\hbar\mu^{-1}\sqrt{2\beta}\right)\right]}{\sqrt{\beta\mu^{-1}}}} \\ & -\frac{\frac{2e^{-\beta V_1}e^{0.5\beta\mu^{-1}\alpha^2\hbar^2}}{\mu}+\frac{2e^{-\beta V_1}e^{0.5\beta\mu^{-1}\left((\alpha\hbar)^{-1}\sqrt{2\mu V_1}-0.5\right)^2}\left((\alpha\hbar)^{-1}\sqrt{2\mu V_1}-0.5\right)}{\mu}}{e^{0.5\beta\mu^{-1}\alpha^2\hbar^2}\left(e^{\left((\alpha\hbar)^{-1}\sqrt{2\mu V_1}-0.5\right)^2}-1\right)+\frac{\sqrt{2\pi}\left[erfi\left(0.5\alpha\hbar\sqrt{2\beta\mu^{-1}}\right)+erfi\left(\left(0.5(\alpha\hbar)^{-1}\sqrt{2\mu V_1}-1\right)\alpha\hbar\mu^{-1}\sqrt{2\beta}\right)\right]}{\alpha\hbar\sqrt{\beta\mu^{-1}}}} \\ & +\frac{V_1\sqrt{2\pi}\left[erfi\left(0.5\alpha\hbar\mu^{-1}\sqrt{2\beta}\right)+erfi\left(\left(0.5(\alpha\hbar)^{-1}\sqrt{2\mu V_1}-1\right)\alpha\hbar\mu^{-1}\sqrt{2\beta}\right)\right]}{e^{0.5\beta\mu^{-1}\alpha^2\hbar^2}\left(e^{\left((\alpha\hbar)^{-1}\sqrt{2\mu V_1}-0.5\right)^2}-1\right)+\frac{\sqrt{2\pi}\left[erfi\left(0.5\alpha\hbar\sqrt{2\beta\mu^{-1}}\right)+erfi\left(\left(0.5(\alpha\hbar)^{-1}\sqrt{2\mu V_1}-1\right)\alpha\hbar\mu^{-1}\sqrt{2\beta}\right)\right]} \end{aligned} \tag{37}$$

$$H_r = RT\frac{315T^3-21T\Theta^2-8\Theta^3}{315T^3+105\Theta T^2+21T\Theta^2+4\Theta T^2}, \tag{38}$$

$$H_t = \frac{5}{2}RT. \tag{39}$$

The R is a universal gas constant whose numeric value equals 8.3144598 J·mol^{-1}·K^{-1}.

Molar entropy

The molar entropy is mathematically given as

$$S = k_\beta T\left(\frac{\partial \ln Q}{\partial T}\right)+k_\beta \ln Q. \tag{40}$$

The molar entropy in Eq. (40) is a contribution of the vibrational, rotational and translational entropies given as

$$S = S_v + S_r + S_t, \tag{41}$$

where the vibrational entropy is

$$
\begin{aligned}
S_v = {} & \frac{K \ln\left\{ e^{0.5\beta\mu^{-1}\alpha^2\hbar^2 - \beta V_1}\left[e^{\left(\alpha^{-1}\hbar^{-1}\sqrt{2\mu V_1}-0.5\right)^2}-1\right] + \frac{\sqrt{2\pi}\left\{erfi\left(0.5\alpha\hbar\sqrt{2\beta\mu^{-1}}\right)+erfi\left(\left((0.5(\alpha\hbar)^{-1}\sqrt{2\mu V_1}-1\right)\alpha\hbar\mu^{-1}\sqrt{2\beta}\right)\right\}}{\alpha\hbar\sqrt{\beta\mu^{-1}}}\right\}}{e^{-\beta V_1}\left\{ e^{0.5\beta\mu^{-1}\alpha^2\hbar^2}\left(e^{\left((\alpha\hbar)^{-1}\sqrt{2\mu V_1}-0.5\right)^2}-1\right) + \frac{\sqrt{2\pi}\left[erfi\left(0.5\alpha\hbar\sqrt{2\beta\mu^{-1}}\right)+erfi\left(\left((0.5(\alpha\hbar)^{-1}\sqrt{2\mu V_1}-1\right)\alpha\hbar\mu^{-1}\sqrt{2\beta}\right)\right]}{\alpha\hbar\sqrt{\beta\mu^{-1}}}\right\}} \\
& + \frac{\frac{V_1\left[e^{0.5\beta\mu^{-1}\alpha^2\hbar^2}\left\{e^{\left(\alpha^{-1}\hbar^{-1}\sqrt{2\mu V_1}-0.5\right)^2}-1\right\}\right] + \frac{\sqrt{2\pi}\left\{erfi\left(0.5\alpha\hbar\sqrt{2\beta\mu^{-1}}\right)+erfi\left(\left((0.5(\alpha\hbar)^{-1}\sqrt{2\mu V_1}-1\right)\alpha\hbar\mu^{-1}\sqrt{2\beta}\right)\right\}}{\alpha\hbar\sqrt{\beta\mu^{-1}}}}{T}}{e^{0.5\beta\mu^{-1}\alpha^2\hbar^2}\left(e^{\left((\alpha\hbar)^{-1}\sqrt{2\mu V_1}-0.5\right)^2}-1\right) + \frac{\sqrt{2\pi}\left[erfi\left(0.5\alpha\hbar\sqrt{2\beta\mu^{-1}}\right)+erfi\left(\left((0.5(\alpha\hbar)^{-1}\sqrt{2\mu V_1}-1\right)\alpha\hbar\mu^{-1}\sqrt{2\beta}\right)\right]}{\alpha\hbar\sqrt{\beta\mu^{-1}}}} \\
& + \frac{\left[\frac{0.5\sqrt{2\pi}\left[erfi\left(0.5\alpha\hbar\sqrt{2\beta\mu^{-1}}\right)+erfi\left(\left((0.5(\alpha\hbar)^{-1}\sqrt{2\mu V_1}-1\right)\alpha\hbar\mu^{-1}\sqrt{2\beta}\right)\right]}{\alpha\hbar\mu T\left(\beta\mu^{-1}\right)^{3/2}} - \frac{0.5\alpha^2\hbar^2 e^{0.5\beta\mu^{-1}\alpha^2\hbar^2}\left\{e^{\left(\alpha^{-1}\hbar^{-1}\sqrt{2\mu V_1}-0.5\right)^2}-1\right\}}{\mu T}\right]}{e^{0.5\beta\mu^{-1}\alpha^2\hbar^2}\left(e^{\left((\alpha\hbar)^{-1}\sqrt{2\mu V_1}-0.5\right)^2}-1\right) + \frac{\sqrt{2\pi}\left[erfi\left(0.5\alpha\hbar\sqrt{2\beta\mu^{-1}}\right)+erfi\left(\left((0.5(\alpha\hbar)^{-1}\sqrt{2\mu V_1}-1\right)\alpha\hbar\mu^{-1}\sqrt{2\beta}\right)\right]}{\alpha\hbar\sqrt{\beta\mu^{-1}}}} \\
& - \frac{\frac{2\alpha\hbar\left(\mu T\sqrt{\beta\mu^{-1}}\right)^{-1}e^{\beta V_1}\left[e^{0.5\beta\mu^{-1}\alpha^2\hbar^2}+\left\{(\alpha\hbar)^{-1}\sqrt{2\mu V_1}-0.5\right\}e^{\alpha^2\hbar^2(0.5(\alpha\hbar)^{-1}\sqrt{2\mu V_1}-1)^2}\right]}{\alpha\hbar\sqrt{\beta\mu^{-1}}}}{e^{0.5\beta\mu^{-1}\alpha^2\hbar^2}\left(e^{\left((\alpha\hbar)^{-1}\sqrt{2\mu V_1}-0.5\right)^2}-1\right) + \frac{\sqrt{2\pi}\left[erfi\left(0.5\alpha\hbar\sqrt{2\beta\mu^{-1}}\right)+erfi\left(\left((0.5(\alpha\hbar)^{-1}\sqrt{2\mu V_1}-1\right)\alpha\hbar\mu^{-1}\sqrt{2\beta}\right)\right]}{\alpha\hbar\sqrt{\beta\mu^{-1}}}}
\end{aligned}
\tag{42}
$$

The rotational entropy is given as

$$S_r = R\left(1 + \ln\left(\frac{T}{\tau\Theta}\right)\right), \tag{43}$$

and the translational entropy is given as

$$S_t = R\left(\frac{5}{2} + \ln\left\{\frac{k_\beta T}{p}\left(\frac{2\pi m}{h^2\beta}\right)^{\frac{3}{2}}\right\}\right), \tag{44}$$

where p is the gas pressure.

Molar Gibbs free energy: The molar Gibbs free energy is given by

$$G = RTV\left(\frac{\ln \partial Q}{\partial V}\right)_T - RT\ln Q. \tag{45}$$

Substituting Eq. (35) into Eq. (45), after some mathematical simplification, the Gibbs free energy in Eq. (45) becomes

$$G = -RT(\ln Q_v + \ln Q_r + \ln Q_t). \tag{46}$$

Molar heat capacity at constant pressure: This is given by

$$C_p = \frac{\partial H}{\partial T}. \tag{47}$$

The heat capacity at constant pressure is a combination of the contributions from vibrational part and the rotational part. The rotational part incorporates the translational part. Hence, the heat capacity at constant pressure becomes

$$C_p = C_v + C_r + \frac{5}{2}R, \tag{48}$$

where

$$C_V = \frac{\partial H_v}{\partial T}, \tag{49}$$

$$C_r = \frac{\partial H_r}{\partial T}. \tag{50}$$

To access the accuracy of the calculated results for the proposed model, we calculate the average absolute percentage deviation using

$$\sigma = \frac{100}{N}\sum\left[(E - C)/E\right], \tag{51}$$

Discussion

In the computation of the numerical values for the four molecules, the value of V_0 is taken as 1 based on the study of Onate et al. in ref[15]. The NIST result represents the experimental data. The four molar thermodynamic properties such as C_p, G, H and S for phosphorous molecule (P_2), potassium molecule (K_2), potassium bromide (KBr) and silicon oxide (SiO) are reported in this study. For numerical computations, we used the following constants: For P_2, $V_1 = 40247.06cm^{-1}$,$\omega_e = 672.20cm^{-1}$, and $\mu = 15.4869amu$. For K_2,$V_1 = 254.0cm^{-1}$, $\omega_e = 21.6324cm^{-1}$, and $\mu = 19.55amu$.For KBr,$V_1 = 2273.91cm^{-1}$,$\omega_e = 196.6cm^{-1}$, and $\mu = 0.0381amu$. For SiO,$V_1 = 66494.76cm^{-1}$,$\omega_e = 1232.51cm^{-1}$, and $\mu = 0.0981amu$. The analytic equations for the molar thermal properties are calculated explicitly in Eqs. (16), (21), (26), and (28) for H, S, G and C_p at constant pressure respectively. The predicted results obtained from the four analytic equations for the four molecules are analyzed in relation to the observed data obtained from NIST[56] data base and reported in Figs. 1, 2, 3 and 4. The effect of temperature on heat capacity at constant pressure for P_2, K_2, KBr and SiO molecules are shown in Figs. 1a, b, c and d respectively. The heat capacity varies smoothly with temperature and shows good agreement between the calculated curves and the NIST data confirming the reliability of the model across the full temperature range (0 to 6000 K). This shows the gradual activation of the rotational and the vibrational degrees of freedom with temperature rise. In Fig. 1(a), there is rapid increase in the heat capacity at low temperatures specifically below 1000 K. Above the 1000 K, the heat capacity grows gradually and approaches a plateau. This reflects that most accessible molecular modes are fully excited. As the vibrational contributions becomes constant, the heat capacity tends to flattening at high temperatures which reflects the characteristic of diatomic molecules. In Fig. 1 (b), an increase in temperature corresponds to a decrease in the heat capacity. The decrease in heat capacity of K_2 with increasing temperature is mainly due to its weak molecular bonding. As temperature rises, the higher vibrational states are rapidly occupied and approach the dissociation limit, leaving few bound states to store additional thermal energy. Consequently, the internal energy becomes less responsive to temperature, leading to a reduction in heat capacity. This behaviour reflects the gradual weakening of the K_2 bond and the onset of thermal dissociation, which is typical for weakly bound alkali dimers. For potassium bromide (KBr) in Fig. 1 (c), a rise in temperature leads to an increase in heat capacity. The variation is smooth

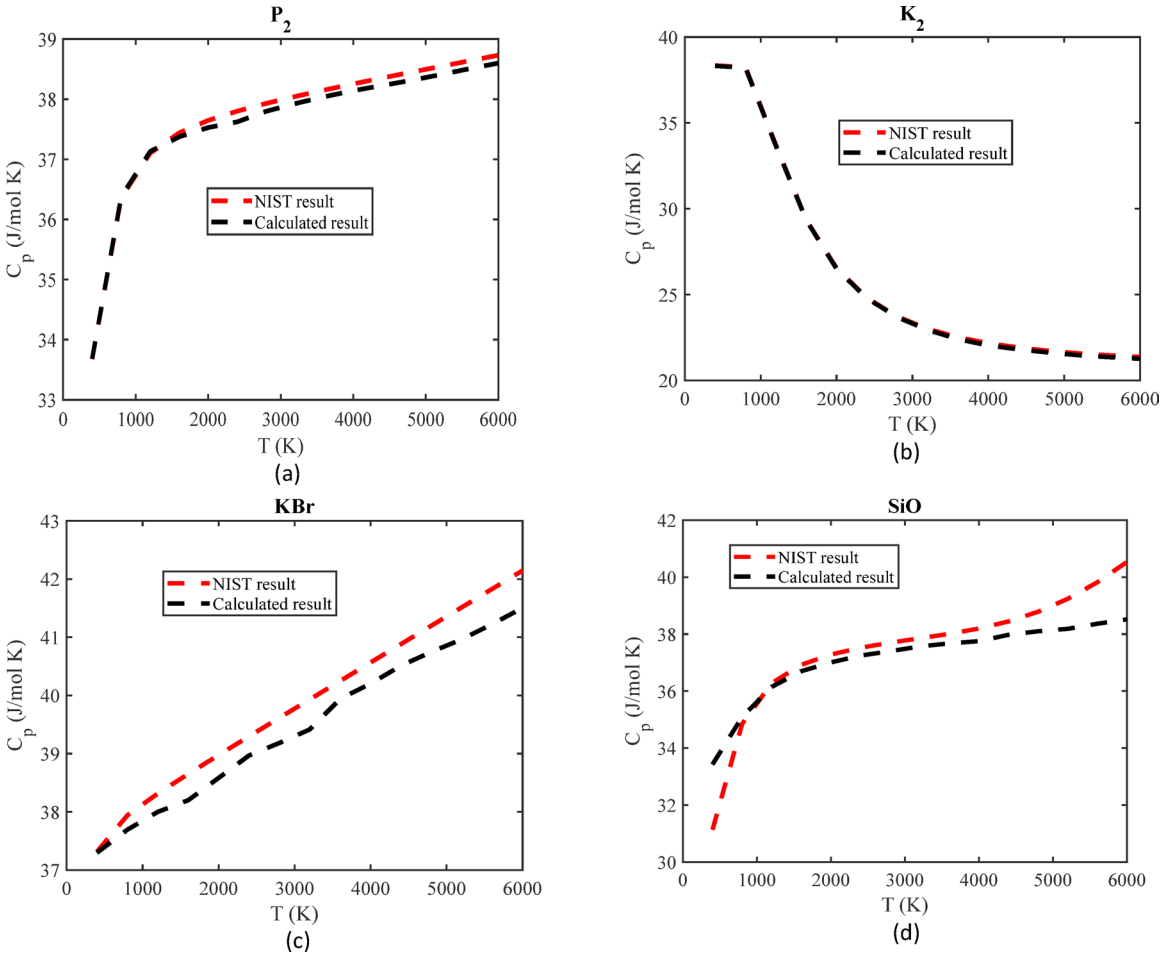

Fig. 1. (**a**): Heat capacity against temperature for phosphorus dimer. (**b**): Heat capacity against temperature for potassium dimer. (**c**): Heat capacity against temperature for potassium bromide. (**d**): Heat capacity against temperature for silicon monoxide.

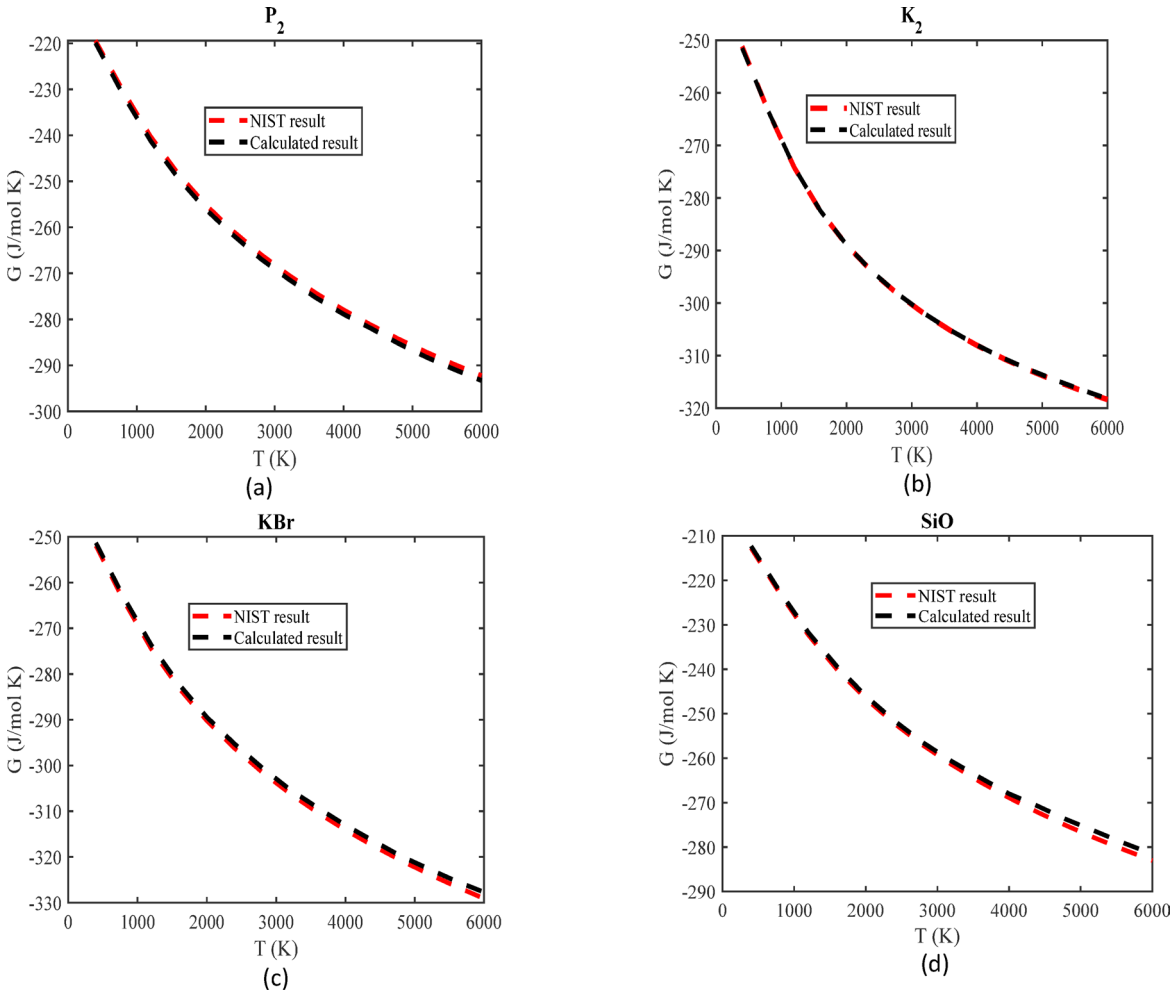

Fig. 2. (**a**): Gibbs free energy against temperature for phosphorus dimer. (**b**): Gibbs free energy against temperature for potassium dimer. (**c**): Gibbs free energy against temperature for potassium bromide. (**d**): Gibbs free energy against temperature for silicon monoxide.

and monotonic as the heat capacity increases slowly with temperature, showing that more vibrational modes get activated at higher temperatures. The rate of increase diminishes slightly at very high temperatures reflecting Dulong-Petit behaviour. KBr is an ionic molecule with stronger binding which maintains increase in thermal capacity as the vibrational modes constantly contributes at high temperatures. In Fig. 1(d), the heat capacity of SiO has a sharp rise at low temperature followed by a gentle saturation at higher temperatures due to a strong covalent bonding. At the initial state, low temperature vibrational activation dominates and high temperature featured quasi-classical. Thus, reflecting typical molecular behaviour where rotational and vibrational modes are increasingly excited with temperature. The analytic Cp for each molecule is consistent with observed data obtained from NIST database. However, the analytic results for each molecule at different temperatures records small disparity from the NIST result. Thus, the average absolute percentage deviation is calculated using Eq. (51) where E stands for the NIST result, C represents the analytic result while N is the number of the observed data. This is to check the overall accuracy of the analytic result for all the temperatures examined. P_2 has deviation of 0.0081%, K_2 has 0.0086, KBr recorded 0.0336% while SiO recorded 0.0246%. The deviations showed that the model has the highest performance for P_2, followed by K_2 then SiO and least KBr. Figure 2 (a, b, c, and d), present Gibbs free energy as a function of temperature for P_2, K_2, KBr and SiO respectively. For all the four molecules, the Gibbs free energy decreases as the temperature rises. This variation justifies the equation $G = H - ST$. The formula shows that an increase in temperature reduces the Gibbs free energy. The decrease is normal as the product of temperature and entropy (T·S) grows larger, making G smaller (becomes more negative). As temperature increases, the G decreases because, the entropy contributions dominate at high temperature. There is a steady variation of the G with temperature. In all the molecules i.e. Figures 2 (a), 2 (b), 2(c), and 2 (d), the analytic Gibbs free energy decreases consistently with increase in temperature. The negativity of the slope indicates that the thermal disorder stabilizes the systems thermodynamically. The closeness of the calculated result to the NIST result demonstrates consistency of the formulation of the partition function. Despite the uniformity in the curves of the four molecules, the typical molecular dimers, P_2 and K_2 show smoother declines while KBr and SiO show stronger curvature. This reflects larger vibrational contributions from ionic/covalent

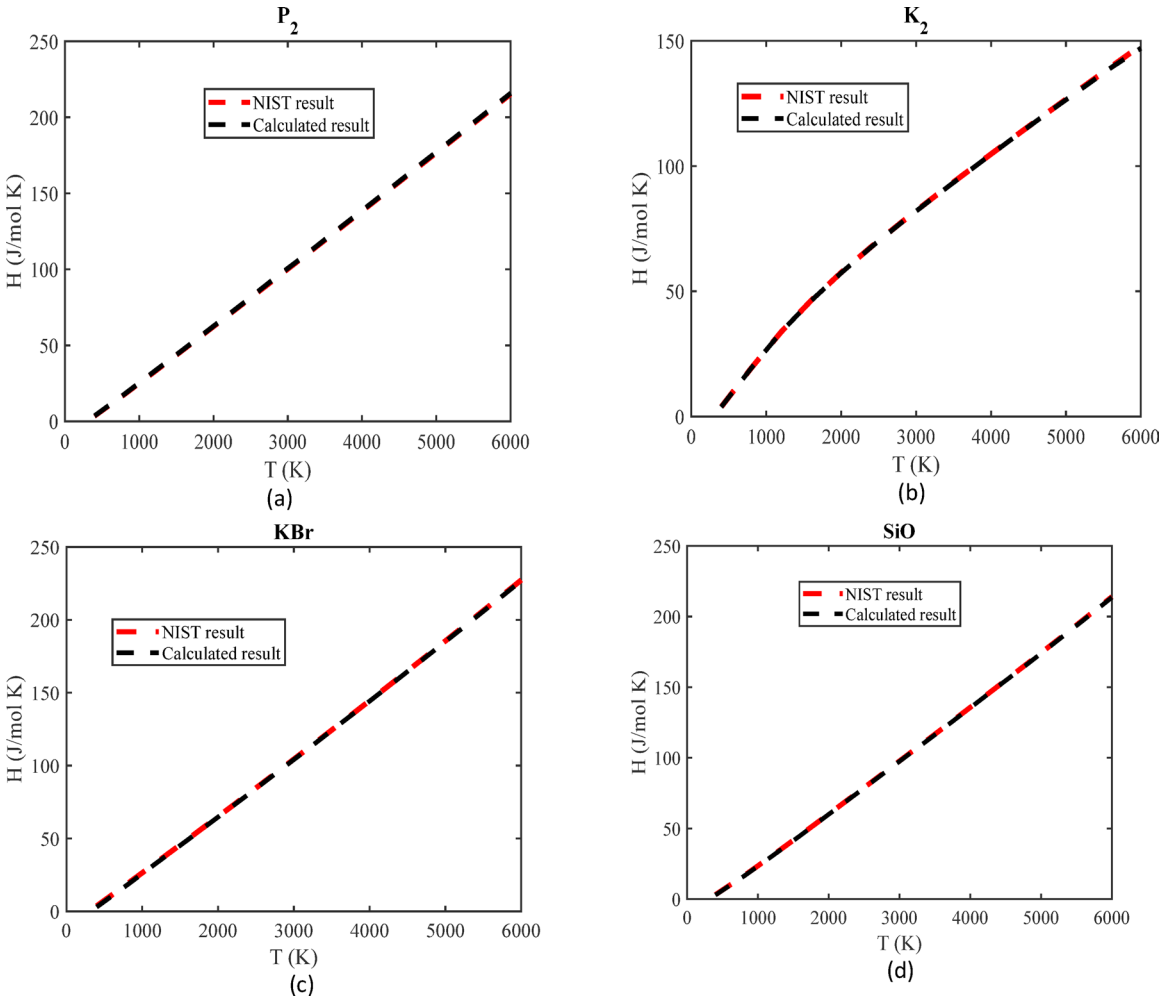

Fig. 3. (**a**): Enthalpy (H) against temperature (T) for phosphorous dimer. (**b**): Enthalpy (H) against temperature (T) for potassium dimer. (**c**): Enthalpy (H) against temperature (T) for potassium bromide. (**d**): Enthalpy (H) against temperature (T) for silicon monoxide.

bonding. The calculated results are found to be in perfect agreement with the observed data (NIST result) for the four molecules studied. However, there are minor differences arising from different model assumptions. Thus, we calculate the average absolute percentage deviation to ascertain the fitness of the model for the various molecules. The average absolution percentage deviation for P_2, K_2, KBr and SiO stand at 0.0110%, 0.0007%, 0.0106% and 0.0119% respectively. This model has the best performance for K_2, followed by KBr, P_2 and finally SiO. In the computation with experimental comparison, the G data obtained from NIST database are scaled relative to a given H data expressed by the equation $G = \frac{-(G_{\exp} - H_{298.15})}{T}$. The $G_{\exp}$ represents the experimentally measured G, while $H_{298.15}$ is the molar enthalpy at $T = 298.15K$ and pressure of 1 bar for gaseous molecules. Thus, the theoretical result of the scaled G is given by $G_{scale} = \frac{-(G - H_{298.15})}{T}$. The G is purely negative for the temperature range of 0 K to 6000 K studied. Figures 3a–c, and d respectively, show the effect of temperature on enthalpy. The Figures indicate that the enthalpy of all four molecules increases almost linearly with temperature and agrees perfectly with the NIST data. This trend is expected since enthalpy is obtained from the temperature integral of the heat capacity. Because the heat capacities change only slightly over the temperature range considered, the enthalpy curves rise in an approximately linear manner. From a physical point of view, this shows that the supplied thermal energy is mainly used to excite translational, rotational, and vibrational motions, without any sudden structural changes or phase transitions. The somewhat steeper slopes observed for KBr and SiO are associated with their higher heat capacities, which result from stronger bonding and greater vibrational contributions. Overall, the smooth increase in enthalpy suggests that energy is absorbed gradually as temperature increases. Due to computational errors, there are small differences between the NIST result and the analytic result, leading to the computations of average absolute percentage deviation. Using Eq. (51), the percentage deviation obtained as 0.0178%, 0.0069%, 0.0129% and 0.0095% for P_2, K_2, KBr and SiO respectively for the enthalpy. Figures 4a–c, and d respectively, illustrate the variation of entropy with temperature for all four molecular systems. The calculated results show good agreement with the NIST data. In each case, entropy increases continuously as temperature rises, which is physically expected since higher thermal energy

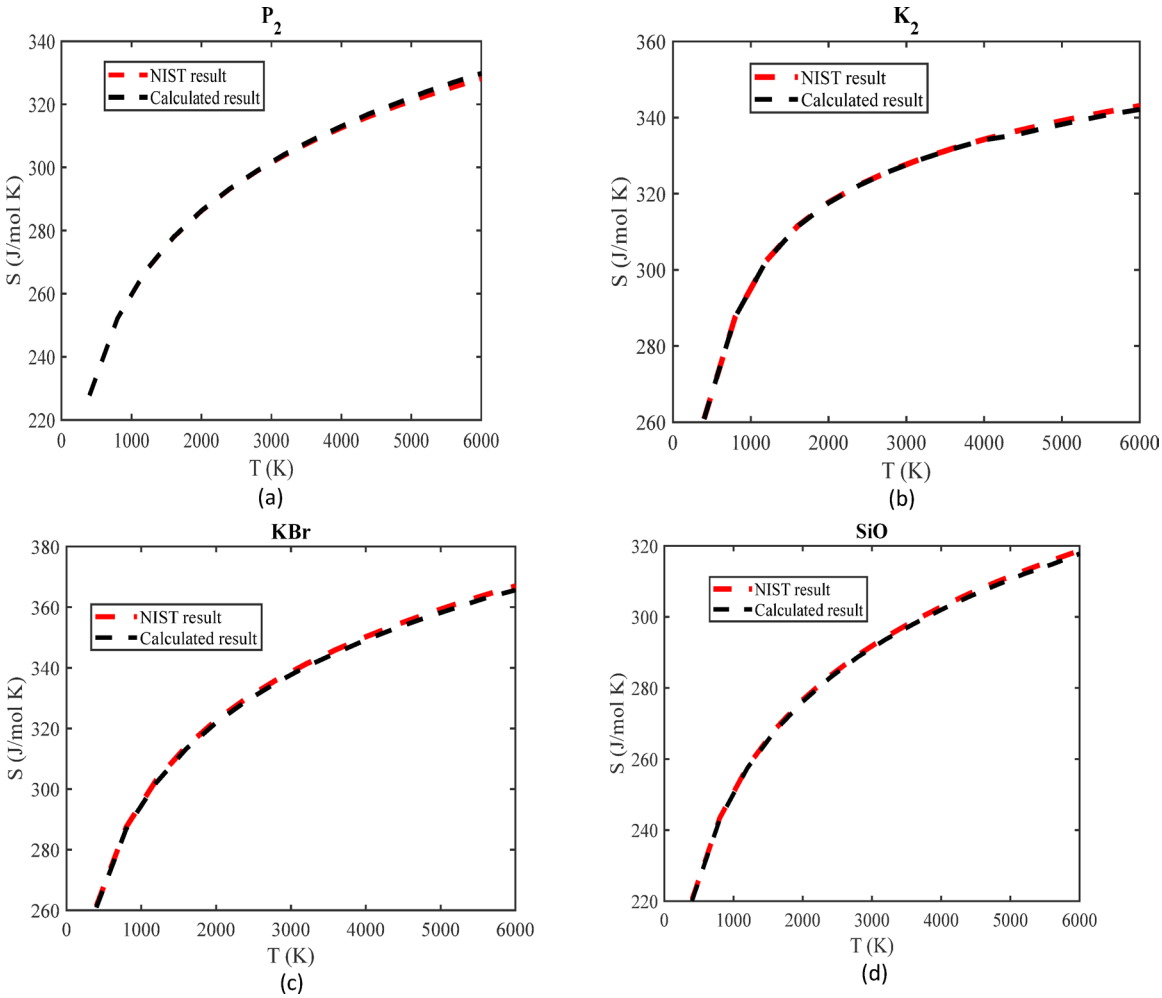

Fig. 4. (**a**): Entropy (S) against temperature (T) for phosphorous dimer. (**b**): Entropy (S) against temperature (T) for potassium dimer. (**c**): Entropy (S) against temperature (T) for potassium bromide. (**d**): Entropy (S) against temperature (T) for silicon monoxide.

α	$I(\rho)$	$I(\gamma)$	$I(\rho)I(\gamma)$
1.0	3.869847	11.849705	45.856548
1.1	2.096430	12.992775	27.238448
1.2	1.484879	13.971001	20.745250
1.3	1.174111	14.816686	17.396430
1.4	0.984967	15.554497	15.320669
1.5	0.856915	16.203493	13.885010
1.6	0.763871	16.778581	12.816677
1.7	0.692773	17.291562	11.979129
1.8	0.636361	17.751885	11.296605
1.9	0.590281	18.167194	10.723743
2.0	0.551763	18.543735	10.231741

Table 1. Fisher information in position space $I(\rho)$and in momentum space $I(\gamma)$ against the screening parameter $\alpha$with $V_0 = 1.2cm^{-1}$ and $V_1 = 0.1cm^{-1}$.

allows the molecules to explore a greater number of accessible microscopic states, thereby increasing disorder in the system. At low temperatures, the entropy increases more rapidly. This initial rise is mainly associated with the activation of rotational and vibrational modes, which are largely frozen out at very low temperatures. As these degrees of freedom become thermally accessible, the number of available molecular configurations grows quickly, leading to a sharp increase in entropy. With further increase in temperature, the growth of entropy becomes more gradual. This slower rise occurs because most of the energetically accessible states are already populated, so additional heating produces only a modest increase in disorder. Differences in entropy among the molecules can be understood in terms of their mass and bonding characteristics. KBr and SiO exhibit relatively higher entropy values, reflecting their heavier masses and stronger vibrational contributions, which provide a

V_1	$I(\rho)$	$I(\gamma)$	$I(\rho)I(\gamma)$
0.1	0.351716	164.69934	57.92740
0.2	0.210199	137.93551	28.99388
0.3	0.163487	124.55179	20.36259
0.4	0.136891	115.90599	15.86643
0.5	0.118544	109.63626	12.99667
0.6	0.104646	104.77582	10.96437
0.7	0.093540	100.83988	9.432516
0.8	0.084356	97.552939	8.229206
0.9	0.076584	94.744351	7.255932
1.0	0.069895	92.301581	6.451409

Table 2. Fisher information in position space $I(\rho)$and in momentum space $I(\gamma)$ against the parameter $V_1$with $\alpha = 0.15cm$and $V_0 = 1.05cm^{-1}$.

V_0	$I(\rho)$	$I(\gamma)$	$I(\rho)I(\gamma)$
1.1	1.196392	63.553611	76.03503
1.2	1.105632	53.402687	59.04371
1.3	0.990734	45.502881	45.08125
1.4	0.863866	39.234627	33.89347
1.5	0.735051	34.177720	25.12238
1.6	0.611771	30.039012	18.37699
1.7	0.499010	26.608951	13.27814
1.8	0.399574	23.734528	9.483706
1.9	0.314533	21.301903	6.700158
2.0	0.243695	19.224967	4.685030

Table 3. Fisher information in position space $I(\rho)$and in momentum space $I(\gamma)$ against the parameter $V_0$with $\alpha = 0.25cm$and $V_1 = 0.15cm^{-1}$.

α	$S(\rho)$	$S(\gamma)$	$S(\rho) + S(\gamma)$
1.0	2.145289	2.171742	4.317031
1.1	1.521436	2.538226	4.059662
1.2	1.195696	2.912732	4.108428
1.3	0.993444	3.289236	4.282680
1.4	0.859292	3.664062	4.523355
1.5	0.768063	4.034935	4.802999
1.6	0.705973	4.400447	5.106420
1.7	0.664591	4.759748	5.424339
1.8	0.638383	5.112349	5.750732
1.9	0.623533	5.458003	6.081536
2.0	0.617320	5.796625	6.413945

Table 4. Shannon entropy in position space $S(\rho)$and in momentum space $S(\gamma)$ against the screening parameter $\alpha$with $V_0 = 1.2cm^{-1}$ and $V_1 = 0.1cm^{-1}$.

V_1	$S(\rho)$	$S(\gamma)$	$S(\rho) + S(\gamma)$
0.1	0.638006	4.573720	5.211725
0.2	2.575030	3.109115	5.684145
0.3	6.157443	2.540851	8.698294
0.4	3.391153	2.228884	5.620037
0.5	2.590704	1.979993	4.570697
0.6	2.123919	1.771104	3.895023
0.7	1.795269	1.590093	3.385361
0.8	1.540743	1.429769	2.970513
0.9	1.331421	1.285502	2.616922
1.0	1.151679	1.154118	2.305797

Table 5. Shannon entropy in position space $S(\rho)$and in momentum space $S(\gamma)$ against the parameter $V_1$with $\alpha = 1.5cm$and $V_0 = 1.05cm^{-1}$.

larger density of states. In contrast, P_2 shows lower entropy due to its lighter mass and simpler molecular structure. Although K_2 is also a diatomic molecule, its weak bonding and anharmonic vibrational behaviour influence how entropy evolves with temperature. Overall, the smooth and monotonic increase of entropy with temperature indicates a gradual population of molecular energy levels, with no evidence of abrupt transitions within the studied range. This behaviour confirms that thermal disorder develops progressively as temperature increases and further supports the consistency of the present theoretical model with standard thermodynamic

V_0	$S(\rho)$	$S(\gamma)$	$S(\rho)+S(\gamma)$
1.1	1.496983	3.490642	4.987626
1.2	1.681436	3.208617	4.890053
1.3	1.871080	2.964353	4.835433
1.4	2.064506	2.751165	4.815671
1.5	2.260310	2.563895	4.824206
1.6	2.457108	2.398497	4.855604
1.7	2.653546	2.251739	4.905285
1.8	2.848318	2.121013	4.969332
1.9	3.040172	2.004182	5.044354
2.0	3.227919	1.899477	5.127396

Table 6. Shannon entropy in position space $S(\rho)$and in momentum space $S(\gamma)$ against the parameter $V_0$with $\alpha = 1.5cm$and $V_1 = 0.15cm^{-1}$.

expectations. Generally, there are computational error, leading to differences between the NIST results and analytic values at each temperature which are very small, suggesting good agreement of the analytic results with the NIST results. The percentage deviation recorded for entropy of the four molecules are 0.0053%, 0.0032%, 0.0092% and 0.0077% for P_2, K_2, KBr and SiO respectively.

Table 1 shows the effect of the screening parameter on both the Fisher information for position space and momentum space. In the position space, an increase in the screening parameter leads to a decrease in the Fisher information, suggesting more delocalization of the wave function in the position space. However, the momentum Fisher information increases as the screening parameter increases, indicating more localization of the wave function. The product of the Fisher information ranges from 10.231741 to 45.856548. The highest product is obtained with the lowest value of the screening parameter, while the lowest product is obtained for the highest value of the screening parameter. The product is a measure related to the uncertainty principle and complexity, and decreases with the screening parameter, reflecting a reduction in the total information with an increase in the screening parameter. The inverse behaviour between the position space and momentum space is consistent with the information trade-off between the position and momentum domains due to Fourier duality. The Fisher information as a function of the screening parameter satisfies both the uncertainty principle and the Cramer–Rao bound. Table 2 shows the effects of the parameter V_1 on both the Fisher information for position space and momentum space. An increase in the parameter V_1 significantly results in a decrease in Fisher information for the momentum space and a slow decrease in the position space. As V_1 increase, the wave function spread over a larger spatial region and becomes smoother. This reduces the magnitude of the spatial gradients of the probability density $\rho(r)$. Since the position-space Fisher information is directly sensitive to the gradients, there is reduction in sharpness and an increase in the delocalization that decreases the Fisher information in the position space. At the same time, the smoother spatial distribution suppresses high-momentum components in the Fourier-transformed wave function. The momentum-space probability density $\gamma(p)$ also becomes smoother, with weaker gradients. Consequently, the momentum-space Fisher information decreases as well. The product of the Fisher information drops sharply, indicating a shift in confinement behaviour due to a changing interaction strength. The high values in the momentum space show a highly localized wave function in the momentum space at low parameter values. Despite the decrease in both spaces, the product of the Fisher information still remains above the minimum. The results in this Table failed to satisfy the uncertainty principle because of the decrease in the conjugate spaces but obeyed the Cramer-Rao inequality since the product of the Fisher information is above the minimum bound. Table 3 shows the effects of the parameter V_0on both the Fisher information for position space and momentum space. The effect of V_0 on the Fisher information is the same as that of V_1on the Fisher information. However, the position space Fisher information with V_0 are higher than the position space Fisher information with V_1. Similarly, the momentum space Fisher information with V_1 are higher than the momentum space Fisher information with V_0. The product of the Fisher information falls rapidly with increasing V_0, suggesting the spread of the wave functions due to a decrease in confinement as the effective potential changes. Table 4 presents Shannon entropy for both the position space and momentum space as a function of the screening parameter. An increase in the screening parameter leads to a decrease in the position space Shannon entropy and an increase in the momentum space Shannon entropy. This shows that the position space wave function becomes more localized with a stronger screening parameter, while the momentum distribution spreads out as a consequence of the uncertainty principle. The sum of the entropies increases monotonically with an increase in the screening parameter, suggesting overall delocalization in the phase space. This characteristic conforms with the entropy-based uncertainty relation known as the Białynicki-Birula and Mycielski (BBM) inequality and indicates that stronger confinement in the position space leads to greater uncertainty in momentum. Table 5 presents the relationship between Shannon entropy in position space and momentum space with the parameter V_1. As V_1increases, both Shannon entropies decrease. This shows that the parameter V_1 has the same sensitivity to both the Shannon entropy for position space and momentum space. Increasing V_1 typically strengthens the attractive part of the interaction or deepens the potential well. This causes the particle to become more tightly bond and makes the wave function concentrate more around the equilibrium region. Thus, the position space probability density becomes narrower which decreases the global spread. This results to decrease in the Shannon entropy for the position space. A stronger confinement in position space generally increases momentum uncertainty. As V_1 increases: the momentum density often becomes more structured and less uniformly spread, making the probability weight concentrates into a smaller effective region of momentum space. This reduces the global disorder of the momentum distribution, leading to decrease in the

Shannon entropy for the momentum space. Despite the decrease in both entropies, the BBM inequality is satisfied even though the uncertainty principle is not obeyed. This also shows that the wave function becomes more sharply localized in the position space and surprisingly concentrated in the momentum space. The behaviour goes against the standard uncertainty trade-off that usually demonstrates localization in one domain leading to spreading in the other. This also shows that the momentum distribution becomes more peaked, indicating that the particle's kinetic energy becomes narrower as the system transits towards more bound-like behaviour. In mathematical terms, the strong confinement causes the wave function to decay more rapidly in space, resulting in a smooth and narrow Fourier transform in the momentum space. The system thus has greater information content with lower uncertainty, making the system more predictable in both the position space and momentum space. As the parameter V_1 increases and the entropies become smaller, quantum fluctuations are suppressed, which may resemble a semiclassical limit where the system acts more classically. Table 6 presents the relationship between Shannon entropy in position space and momentum space with the parameter V_0. An increase in V_0 leads to an increase in the position space but a decrease in the momentum space. This shows that a localized density function corresponds to a delocalized density function. This aligns with the usual entropic behaviour for normal systems. The Shannon entropy here captures global uncertainty and exhibits complementary behaviour in the position space and momentum space.

Conclusion

This study developed accurate analytic models for the information theory and molar thermodynamic properties. The analytic equations for the Fisher information and Shannon entropy incorporate the parameters of the model. The results for the Fisher information and Shannon entropy proved the validity of the model in the study of information theory since the quantities exhibited consistent duality between position and momentum spaces, reflecting uncertainty principle and offering insight to the localization and delocalization of molecular wave functions. The molar thermodynamic properties like Cp, G, H, and S are applied to some molecules such as P_2, K_2, KBr, and SiO molecules over a temperature range of 0 K to 6000 K. The analytic results show strong agreement with experimental data from the NIST database, with average absolute percentage deviations within the acceptable bounds. The thermal behaviour of each molecule was interpreted based on its structural and spectroscopic characteristics, highlighting phenomena such as vibrational saturation and anharmonicity in K_2. These results confirm the robustness of the modeling approach and its capability to accurately describe molecular thermodynamic behaviour across a broad temperature spectrum. However, some minor discrepancies were observed at different temperatures, which may be due to approximations in vibrational, rotational, or electronic contributions not fully captured in the analytic expressions. However, the models assume ideal gas behaviour, which may not hold under high pressure or condensed phase conditions. This model performs better for phosphorous dimer than the modified hyperbolical-type potential reported in ref[57]. for the four thermal properties. While the present model recorded deviation of 0.053%, 0.0178%, 0.0110% and 0.0081% for entropy, enthalpy, Gibbs free energy and heat capacity of P_2, the modified hyperbolical-type model recorded 0.3795%, 0.8939%, 0.3895, and 0.6978%.

Data availability

The datasets used and/or analysed during the current study available from the corresponding author on reasonable request.

Received: 30 September 2025; Accepted: 11 March 2026
Published online: 20 March 2026

References

1. Shannon, C. E. A mathematical theory of communication. *Bell Syst. Tech. J.* **27**, 623–656 (1948).
2. Shannon, C. E. & Weaver, W. *The Mathematical Theory of Communication* (University of Illinois Press, 1949).
3. Abdushukurov, A., Nurmukhamedova, N. & Abdushukurov, F. On Fisher–Bhattacharyya information function and lower bounds under right random censoring. *Lobachevskii J. Mathematics.* **45**, 4846–4857 (2024).
4. Amadi, P. O. et al. Information entropies for H_2 and ScF diatomic molecules with Deng-Fan-Eckart potential. *Revista Mex Fisica*. **66**, 742–748 (2020).
5. Cover, T. M. & Thomas, J. A. *Elements of information theory* 2nd Edition. (2006).
6. Dehesa, J. S., Koga, T., Yanez, R. J., Plastino, A. R. & Esquivel, R. O. Quantum entanglement in helium. *J. Phys. B: At. Mol. Opt. Phys.* **45**, 015504 (2012).
7. Sanchez-Moreno, P., Plastino, A. R. & Dehesa, J. S. A quantum uncertainty relation based on Fisher's information. *J. Phys. A: Math. Theor.* **44**, 065301 (2011).
8. Moses, S. A. et al. D.S. Creation of a low-entropy quantum gas of polar molecules in an optical lattice. *Science* **350**, 659–662 (2015).
9. Yunus, N. M., Mutalib, M. I. A., Man, Z., Bustam, M. A. & Murugesan, T. Solubility of CO_2 in pyridinium based ionic liquids. *Chem. Eng. J.* **189**, 94–100 (2012).
10. Rahmatov B., Turimov B., Murodov S., Xaknazarova X., Usanov S., Vapayev M., Avezmuratova Z. Magnetic field by current loop in the Janis-Newman-Winicour spacetime. *Nuclear Physics B* **6**, 117344 (2026)
11. Maurya, S. K., Bouzenada, A., Ashraf, A., Ray, S., Alqahtani, A., Saidov, I., Atamurotov, F. Exploring the effect of inverse electrodynamics on charged black holes through oscillatory motion and collisions. *Annals of Physics* **488**, 170417 (2026)
12. Amano, K. I., Yoshidome, T., Harano, Y., Oda, K. & Kinoshita, M. Theoretical analysis on thermal stability of a protein focused on the water entropy. *Chem. Phys. Lett.* **474**, 190–194 (2009).
13. Satpalthy, A. & Satpathy, S. A model evaluation of entropies and related thermal quantities of alkali halides based on a generalised bonding scheme. *Indian J. Phys.* **98**, 3865–3875 (2024).
14. Gopala, R. V. & Satpathy, A. On the evaluation of entropy and thermodynamic properties of 1:1 type of molten salts through the generalized Debye inverse screening length. *Pss(b)*: 150, 53–58 (1988).
15. Eyube, E. S., Notani, P. P. & Samaila, H. Analytical prediction of enthalpy and Gibbs free energy of gaseous molecules. *Chem. Thermody Therm. Anal.* **6**, 100060 (2022).

16. Emeje, K. O., Aghemenloh, E. & Onate, C. A. Analytical determination of enthalpy, heat capacity and Gibbs free energy for nitrogen and iodine. *Chem. Phys. Lett.* **844**, 141271 (2024).
17. Horchani, R. & Jelassi, H. Accurate and general model to predict molar entropy for diatomic molecules. *South. Afr. J. Chem. Engr.* **33**, 103–106 (2020).
18. Horchani, R., Al Shafii, S., Friha, H. & Jelassi, H. A Straightforward Model for Molar Enthalpy Prediction of CsO, CsF, and CsCl Molecules Via Shifted Tietz-Wei Potential. *Int. J. Thermophys.* **42**, 84 (2021).
19. Jia, C-S. et al. Prediction of entropy and Gibbs free energy for nitrogen. *Chem. Eng. Sci.* **202**, 70 (2019).
20. Onate, C. A. et al. Theoretical prediction of molar entropy of modified shifted Morse potential for gaseous molecules. *Chem. Phys.* **582**, 112294 (2024).
21. Onate, C. A. et al. Molar enthalpy and heat capacity for symmetric trigonometric Rosen-Morse plus Pöschl-Teller potential. *South. Afr. J. Chem. Eng.* **51**, 15–21 (2025).
22. Ren, D. et al. Harmonizing physical and deep learning modeling: A computationally efficient and interpretable approach for property prediction. *Scripta Mater.* **255**, 116350 (2025).
23. Xu, X., Hu, Y., He, Y., Han, J. & Zhu, J. High-order analysis of lattice Boltzmann models for the conservative Allen-Cahn equation. *Comput. Math Appl.* **146**, 106–125 (2023).
24. Onate, C. A. et al. Vibrational spectra for an extended cosine hyperbolic type potential model. *Results Chem.* **14**, 102110 (2025).
25. Horchani, R. et al. Relativistic bound state solutions and quantum information theory in D dimensions under exponential-type plus Yukawa potentials. *Sci. Rep.* **14**, 28582 (2024).
26. Omugbe, E. et al. The correspondences between variance and information entropies of a particle confined by a q-deformed hyperbolic potential. *Mod. Phys. Lett.* **A 39**, 2450151 (2024).
27. Onate, C. A. et al. Eigensolutions and quantum fisher information for different potential models. *AVS Quantum Sci.* **5**, 025003 (2023).
28. Omugbe, E. et al. Expectation values and Fisher information theoretic measures of heavy flavoured mesons. *J. Nig Soc. Phys. Sci.* **7**, 2350 (2025).
29. Chen, W-L. et al. Fisher and Shannon information entropies in 2-dimension for a non-central potential as applied to hydrogen diatomic molecules. *Results Phys.* **75**, 108303 (2025).
30. Hsu, C-Y. et al. A.A. Information theory and thermodynamic study of a 2D harmonic oscillator modified by inverse square potential. *Sci. Rep.* https://doi.org/10.1038/s41598-025-33259-1 (2025).
31. Idiodi, J. O. A., Onate, C. A. & Entropy Fisher Information and Variance with Frost-Musulin Potenial. *Commun. Theor. Phys.* **66**, 269–274 (2016).
32. Onate, C. A., Ikot, A. N., Onyeaju, M. C., Ebomwonyi, O. & Idiodi, J. O. A. Effect of dissociation energy on Shannon and Rényi entropies. *Karbala Int. J. Mod. Sci.* **4**, 134–142 (2018).
33. Wu, X., Zhao, Y. A. & Novel Heat Pulse Method in Determining Effective Thermal Properties in Frozen Soil. *Water Resour. Res.* **60**, (2024).
34. Xia, G., He, X., Jia, Y., Zhu, Y. & Tian, Z. Design of a Cylindrical Thermal Rotary Concentrator Based on Transformation Thermodynamics. *Materials* **18**, 4440 (2025).
35. Onate, C. A., Deji-Jinadu, B. B., Ajani, O. O., Akinpelu, J. A. & Adeniji, A. A. Bound states and vibrational thermodynamic properties of scarf type potential model. *J. Low Temp. Phys.* https://doi.org/10.1007/s10909-024-03177-z (2024).
36. Ahmed, A. D., Eyube, E. S., Omugbe, E., Onate, C. A. & Timtere, P. Bound-state energy spectrum and thermochemical functions of the deformed Schiöberg oscillator. *Sci. Rep.* **13**, 20386 (2023).
37. Onate, C. A. et al. Theoretic measure and thermal properties of a standard Morse potential model. *J. Mol. Mod* **29**, 34 (2023).
38. Inyang, E. P. et al. Analytical solutions of the N-dimensional Schrodinger equation with modified screened Kratzer plus inversely quadratic Yukawa potential and thermodynamic properties of selected diatomic molecules. *Results Phys.* **43**, 106075 (2022).
39. Isonguyo, C. N. et al. Eigensolutions and Thermodynamic Properties of Kratzer Plus Generalized Morse Potential. *Front. Phys.* **10**, 962717 (2022).
40. Peng, X-L., Jiang, R., Jia, C-S., Zhang, L-H. & Zhao, Y-L. Gibbs free energy of gaseous phosphorus dimer. *Chem. Eng. Sci.* **190**, 122 (2018).
41. Jia, C-S. et al. Predictions of entropy for diatomic molecules and gaseous substances. *Chem. Phys. Lett.* **692**, 57 (2018).
42. Onate, C. A. et al. Shannon entropy and thermodynamic properties of an inversely quadratic Yukawa potential model. *J. Nig. Soc. Phys. Sci.* **6**, 2134 (2024).
43. Onate, C. A., Adedewe, O., Ikubanni, S. O. & Olanrewaju, D. B. Spectral and thermodynamic properties of a particle in multiparameter exponential-type radial potential. *Low Temp. Phys.* **50**, 1168 (2024).
44. Onate, C. A. et al. O.E.O. Thermodynamic properties for a combination of Varshni and Coulomb potentials. *Therm. Adv.* **1**, 100001 (2024).
45. Onate, C. A., Okon, I. B., Omugbe, E., Eyube, E. S. & Emeje, K. O. Thermodynamic properties and the confinement frequency for Second Pöschl-Teller potential. *Results Phys.* **70**, 108144 (2025).
46. Liu, G-H., Ding, Q-C., Wang, C-W. & Jia, C-S. Unified non-fitting explicit formulation of thermodynamic properties for five compounds. *J. Mol. Str.* **1294**, 136543 (2023).
47. Dong, S-H., Lemus, R. & Frank, A. Ladder operators for the Morse potential. *Int. J. Quant. Chem.* **86**, 433–439 (2002).
48. Dong, S-H. The SU (2) realization for the Morse potential and its coherent states. *Can. J. Phys.* **80**, 129 (2002).
49. Dong, S-H. & Cruz-Irisson, M. Energy spectrum for a modified Rosen-Morse potential solved by proper quantization rule and its thermodynamic properties. *J. Math. Chem.* **50**, 881–892 (2002).
50. Dong, S-H., Lozada-Cassou, M., Jimenze-Ángeles, Y. U. J., Rivera, A. L. & F. and Hidden symmetries and thermodynamic properties for a harmonic oscillator plus an inverse square potential. *Int. J. Quant. Chem.* **107**, 366–371 (2007).
51. Khordad, R. & Sedehi, H. R. R. Thermodynamic properties of a double ring-shaped quantum dot at low and high temperatures. *J. Low Temp. Phys.* **190**, 200–212 (2018).
52. Khordad, R. & Ghanbari, A. Theoretical prediction of thermodynamic functions of TiC: Morse ring-shaped potential. *J. Low Temp. Phys.* **199**, 1198–1210 (2020).
53. Khordad, R. & Ghanbari, A. Analytical calculations of thermodynamic functions of lithium dimer using modified Tietz and Badawi-Bessis-Bessis potentials. *Comput. Theor. Chem.* **1155**, 1–8 (2019).
54. Strekalov, M. An accurate closed-form expression for the partition function of Morse oscillators. *Chem. Phys. Lett.* **439**, 209–212 (2007).
55. Onate, C. A., Deji-jinadu, B. B., Ajani, O. O., Akinpelu, J. A. & Ebomwonyi, O. Information theory and thermodynamic properties for a combined potential model. *Sci. Rep.* **15**, 2626 (2025).
56. NIST (National Institute of Standards and Technology) & Chemistry WebBook, N. I. S. T. *NIST Standard Ref. Database Number* **69** https://doi.org/10.18434/T42S31 (2017).
57. Eyube, E. S. Prediction of thermal properties of phosphorus dimer-the analytical approach. *Chem. Phys. Lett.* **801**, 139702 (2022).

Acknowledgements

The author Ali A. Rajhi extends his appreciation to the Deanship of Scientific Research at King Khalid University, Saudi Arabia for funding this work through Small Research Group Program under Grant No. RGP. 1/84/46.

Author contributions

Conceptualization, Supervision : Pradeep Kumar Singh***Formal Analysis*** : Makus Ahmes, Chou-Yi Hsu and Yusufbay Yusupov***Software: *** Ibrahim Mahariq***Writing original draft*** : Doniyor Jumanazarovh.

Declarations

Competing interests

The authors declare no competing interests.

Additional information

Correspondence and requests for materials should be addressed to P.K.S. or M.A.

Reprints and permissions information is available at www.nature.com/reprints.

Publisher's note Springer Nature remains neutral with regard to jurisdictional claims in published maps and institutional affiliations.